

Ground and Excited Electronic Structures of Electride and Alkalide Units: The Cases of Metal-Tren, -Azacryptand, and -TriPip222 Complexes

Isuru R. Ariyaratna

Department of Chemistry and Biochemistry, Auburn University, Auburn, AL 36849-5312, USA

Abstract

A systematic electronic structure analysis was conducted for $M(L)_n$ molecular electrifieds and their corresponding alkalide units $M(L)_n@M'$ ($M/M' = Na, K$; $L = Tren, Azacryptand, TriPip222$; $n = 1, 2$). All complexes belong to the “superalkali” category owing to their low ionization potentials. The saturated molecular electrifieds display $M^+(L)_n^-$ form with a greatly diffused quasispherical electron cloud. They were identified as “superatoms” considering the contours of populating atomic-type molecular orbitals. The observed superatomic Aufbau order of $M(Tren)_2$ is 1S, 1P, 1D, 1F, 2S, 2P, and 1G and it is consistent with those of $M(Azacryptand)$ and $M(TriPip222)$ up to the analyzed 1F level. Their excitation energies decrease gradually moving from $M(Tren)_2$ to $M(Azacryptand)$ and to $M(TriPip222)$. The studied alkalide complexes carry $[M(L)_n]^+@M'^-$ ionic structure and their dissociation energies vary in the sequence of $K(L)_n@Na > Na(L)_n@Na > K(L)_n@K > Na(L)_n@K$. Similar to molecular electrifieds, the anions of alkalide units occupy electrons in diffuse Rydberg-like orbitals. In this work, excited states of $[M(L)_n@M']^{0/+/-}$ and their trends are also analyzed.

I. Introduction

Electrides are truly unique in the sense that electron localization is found in lattice voids rather than in the vicinity of cationic metal centers. Hence deservingly, electrides and its akin alkalides have attracted a notable attention over the years (see Refs. 1–5 and references therein). An electride is simply an outcome of metal atom coordination with particular ligands that prompts spontaneous metal-to-interstitial electron transfers.^{1,2} On the contrary, in alkalides the anionic interstitial sites are populated by alkali metal atoms in the form of anions, i.e., Na⁻, K⁻, Rb⁻, or Cs⁻.^{5,6} Electrons of alkalides are weakly bound to the crystalline framework similar to electrides due to the lower electron affinity of interstitial alkali metal atoms.⁷ Such unique electron arrangements endow electrides and alkalides with properties such as low work function,⁸ antiferromagnetism,⁹ strong reducing power,^{4,10–12} and high hyperpolarizability.^{13,14} Hence, they are potential candidates in catalysis, optics, electronics, and magnetic materials related applications.^{4,5,13,15,16}

Despite a variety of electrides and alkalides being discovered in ambient conditions, their experimental analysis bear challenges due to their low stability. Consequently, computational tools have been a preferred method to shed light on their properties.^{3,4,17–21} Notably, such techniques are used to confirm the existence of interstitial electrons in electrides¹⁷ and ion pairing in alkalide solutions.¹⁰ Furthermore, theoretical studies of precursors of electrides and alkalides provide insight on their electronic structures enabling progress in designing, property tuning, and potential synthesizing of desirable electron rich materials.^{10,22–25}

The building blocks of saturated organic electrides themselves are a fascinating class of complexes with unique electronic structures. For example, units such as Na(15-Crown-5), K(18-Crown-6), Na[2.2.2]cryptand, and K[2.2.2]cryptand possess a quasispherical highly diffused electron cloud in the periphery (like an s-orbital) with an ionic structure.^{22,23} Even more interestingly these complexes populate atomic p-, d-, f-type orbitals (or superatomic (SA) P-, D-, F-orbitals) in excited states, and hence are identified as “Superatoms”. Our past attempts disclosed their Aufbau shell model, which is chiefly 1S, 1P, 1D, 1F, 2S, and 2P (in some instances 2S populates prior to the 1F).^{22,23} Similar orders are observed in a series of other Rydberg-like systems as well, namely, endohedral M@C₂₀H₂₀ (M = Li, Na, K, Rb),^{26,27}

$M(\text{NH}_3)_4$ ($M = \text{Li}, \text{Na}$),²⁸ and $M(\text{H}_2\text{O})_6$ ($M = \text{Mg}^+, \text{Ca}^+$).^{29,30} Complexes with such expanded electron clouds tend to carry extremely low ionization potentials and can also be recognized as “Superalkalis”.^{31,32}

In the present work ground and electronically excited states of metal-coordinated Tris(2-aminoethyl)amine (Tren), Azacryptand (Azacrypt),³³ and TriPip222 cryptand (Tripip)³⁴ molecular electriles and their corresponding alkalide units are investigated. Due to the comparable ligand architecture and the identical coordination number, the $M(\text{L})_n$ electrile and $M(\text{L})_n@M'$ alkalide systems ($M/M' = \text{Na}, \text{K}$; $L = \text{Tren}, \text{Azacrypt}, \text{Tripip}$; $n = 1, 2$) provide particularly useful information for their fundamental property comparisons. This article highlights their geometric features, chelation strengths, and electron ionizations and transitions. Furthermore, their SA nature originating from the shapes of the molecular orbitals and the smaller ionization potentials are discussed in detail. In this regard, their ground state geometries, dissociation energies (D_{es}), ionization energies (IEs), and excitation energies are obtained using DFT (density functional theory), MP2 (Møller–Plesset second-order perturbation theory), and EPT (electron propagator theory) and are discussed in following sections.

II. Computational details

The geometries of all reported species were optimized at the DFT/CAM-B3LYP³⁵ level using correlation-consistent double- ζ quality aug-cc-pVDZ basis set.^{36,37} At the same basis set structures were reoptimized using the DFT/B3LYP³⁸⁻⁴¹ and followed by harmonic vibrational frequency calculations to confirm their existence on the potential energy surface. Cartesian coordinates and the harmonic vibrational frequencies of optimized complexes are reported in the Supporting Information (SI). At the DFT/CAM-B3LYP level, D_{e} of all focused molecular electriles and their cations were calculated with respect to $M(\text{L})_n^{0,+} \rightarrow M^{0,+} + nL$, when all fragments are at their ground electronic states ($M = \text{alkali metal}, L = \text{chelating ligand}, n = 1, 2$). The D_{es} of the focused alkalide units and their cations were calculated with respect to $[M(\text{L})_n@M']^{0,+} \rightarrow [M(\text{L})_n]^{0,+} + M'$ ($M' = \text{external alkali metal atom}$) fragmentation. At the same level of theory, adiabatic ionization energies (AIEs) of all species were collected. Utilizing the same basis set, single-point MP2⁴² calculations were also performed for the

CAM-B3LYP geometries of neutral and cationic $\text{Na}(\text{Tren})_2@Na$, $\text{Na}(\text{Tren})_2@K$, and $K(\text{Tren})_2@Na$, to obtain more accurate D_{es} and AIEs. The spin contamination associated with the unrestricted Hartree–Fock wave functions of open-shell complexes is minor.

The vertical electron attachment energies (VEAEs) of $M(\text{Tren})_{1,2}^+$, $M(\text{Azacrypt})^+$, and $M(\text{Tripip})^+$ were calculated using the EPT, i.e., Koopmans’s theorem (KT), diagonal second-order (D2), partial third-order quasiparticle (P3), and renormalized partial third-order quasiparticle (P3+) methods,^{43–47} using the double- ζ quality cc-pVDZ (M, C, N) d-aug-cc-pVDZ (H) basis set. These EPT calculations were performed using the geometries of the neutral complexes. The excitation energies of the neutral complexes were inferred from the differences of the VEAEs of the cations (see Refs. 45–47 for more information). The D2 VEAEs of $[M(L)_n@M']^{2+}$ and $M(L)_n@M'$ were computed using the $[M(L)_n@M']^+$ and $[M(L)_n@M']^-$ geometries with the aug-cc-pVDZ basis set for all atoms, to analyze their low-lying electronic states. Furthermore, at the same level of theory vertical singlet-triplet energy gaps (ΔE_{s-t}) of $M(L)_n@M'$ were obtained at the geometry of singlet spin structures. For all EPT calculations CAM-B3LYP geometries were used. In all cases, pole strengths corresponding to the VEAEs are larger than 0.85 and, hence excitation energies are reliable. Calculated VEAEs and the corresponding pole strengths of all species are reported in the SI.

All calculations were performed using the Gaussian 16 suite. IboView,⁴⁸ Molden,⁴⁹ and GaussView⁵⁰ software packages were used to produce molecular orbitals.

III. Results and discussion

IIIA. $M(\text{Tren})_{1,2}$, $M(\text{Azacrypt})$, and $M(\text{Tripip})$ ($M = Na, K$) complexes

The polarization of valence ns^1 electron of M ($M = Na, K$) facilitates an efficient dative attack from the Tren ligand by minimizing the metal-ligand electron-electron repulsion (see the molecular orbital of $\text{Na}(\text{Tren})$ in Figure 1). The chelation of $M(\text{Tren})$ with another Tren ligand forces the valence electron to the periphery of the complex (compare the orbitals of $\text{Na}(\text{Tren})$ and $\text{Na}(\text{Tren})_2$ in Figure 1). $\text{Na}(\text{Tren})$ can be recognized as “quasi-valence-type” based on the high electron localization on the metal center, whereas $\text{Na}(\text{Tren})_2$ is a “surface-type” complex as a result of its distributed peripheral electron cloud (see Refs. 51,52 for

more information on this terminology). In ground states, all studied $M(\text{Tren})_2$, $M(\text{Azacrypt})$, and $M(\text{Tripip})$ ($M = \text{Na}, \text{K}$) systems carry an expanded electron cloud and hence they belong to the surface-type category. An accurate representation of this diffuse electron cloud is vital for analyzing their geometries.^{23,29,30} Specifically, the implemented CAM-B3LYP method with a diffuse basis set in this work has been proven to produce accurate geometries on them.⁵³ Surface-type structures are known to have longer N–H and shorter M–N bonds due to the $\text{N}^{\delta-}-\text{H}^{\delta+}$ and $\text{M}^{\delta+}-\text{N}^{\delta-}$ charge localization. Specifically, the exterior electron cloud attracts the $\delta+$ charged H–atoms which stretches N–H bonds whereas its repulsion with the $\delta-$ charged N–atoms compresses the M–N bonds (see Refs. 28,54). These patterns are preserved by the systems described in this work (compare the slightly longer N–H and shorter M– N_e (N_e = equatorial N-atoms) bonds of neutral systems compared to their cations listed in Table 1). Note that the interaction of N-atoms in the equatorial positions with the doughnut-shaped diffuse electron cloud is greater compared to the axial N-atoms (Figure 1) and hence the pattern is not maintained in M– N_a (N_a = axial N-atoms) bonds (Table 1).

Generally, as we move down of the periodic table the D_e s of alkali metal-complexes decrease.^{23,55,56} This is in line with all the studied systems in this work except for $\text{Na}(\text{Azacrypt})$ which has a 4.47 kcal/mol lower D_e compared to $\text{K}(\text{Azacrypt})$ (see Table 1). The total number of coordination sites of each $M(\text{Tren})_2$, $M(\text{Azacrypt})$, and $M(\text{Tripip})$ complex is eight and their D_e s are comparable. Among the neutral complexes the largest D_e s were observed for $M(\text{Tren})_2$ whereas the comparatively lesser D_e s of $M(\text{Azacrypt})$ and $M(\text{Tripip})$ may be a result of the combination of the higher stress of bonds in their cage-type structures and the diffuse electron cloud. Upon comparing the cage-type structures, the $\text{Na}(\text{Tripip})^{0,+}$ show higher D_e s compared to $\text{Na}(\text{Azacrypt})^{0,+}$ whereas the opposite is true for $\text{K}(\text{Tripip})^{0,+}$ vs. $\text{K}(\text{Azacrypt})^{0,+}$. In all cases the cationic complexes carry larger D_e s compared to the neutral complexes owing to the stronger electrostatic attraction between M^+ and electron rich ligands.

The IEs of surface-type complexes are lower compared to the quasi-valence-type structures,^{30,57,58} which is further corroborated by this work, i.e., the AIEs and VIEs (vertical IEs) of $M(\text{Tren})_2$ are 0.5–0.6 eV smaller compared to the $M(\text{Tren})$ at all levels of theory (Table 1). Note that the D2, P3, and P3+ VIEs were obtained by calculating –VEAEs of the cationic systems using the geometries of their neutral structures. VIEs obtained at D2, P3, and P3+

levels agree within 0–0.007 eV. The IEs decrease in the order of $M(\text{Tren})_2 > M(\text{Azacrypt}) > M(\text{Tripip})$ and the pattern correlates to the number of N–H terminals of the complexes. This highlights the importance of N–H terminals (rather than the number of C–H terminals) on the stabilization of the diffuse electron cloud against the ionization. All studied Na-complexes carry larger IEs compared to their corresponding K-complexes. Notice that the IEs of Na (5.139 eV) and K (4.341 eV) atoms are more than twice as high compared to the IEs of the corresponding complexes.⁷ Indeed, the IEs of all studied complexes are smaller than that of any atom in the periodic table and hence can be recognized as “superalkalis”.³¹ The chelating ligand of the previously studied Na[2.2.2]cryptand has a denticity of eight similar to Azacrypt and Tripip ligands, and the structure of Na[2.2.2]cryptand closely resembles the Na(Azacrypt) where the O-atoms of the former is replaced by N–H in the latter.^{23,59} The reported D2 VIE of Na[2.2.2]cryptand is 1.669 eV which is lower by 0.099 eV from value of the Na(Azacrypt) and interestingly closer to that of K(Tripip), i.e., 1.694 eV.

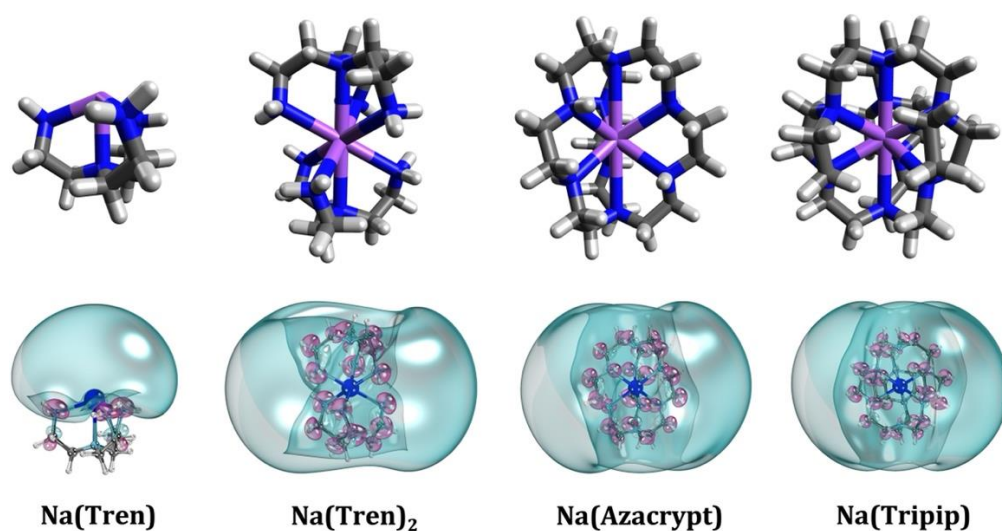


Figure 1. Geometries (top-row) and the contours of singly occupied molecular orbitals (bottom-row) of $\text{Na}(\text{Tren})_{n=1,2}$, $\text{Na}(\text{Azacrypt})$, and $\text{Na}(\text{Tripip})$ complexes. A threshold of 70% was used. Structures and the orbital contours of corresponding potassium complexes have similar shapes.

Table 1. Point group symmetries, dissociation energies (D_e , kcal/mol), adiabatic ionization energies (AIE, eV), vertical ionization energies (VIE, eV), and equilibrium M–N and N–H bond distances (r_e , Å) of $M(L)_n^{0,+}$ systems.

Species	Point group	D_e	AIE	VIE			r_e^a		
				D2	P3	P3+	M–N _e	M–N _a	N–H
Na(Tren)	C ₃	21.33	2.689	2.613	2.618	2.618	2.460	2.640	1.019
Na(Tren) ⁺	C ₃	82.98					2.432	2.421	1.018
K(Tren)	C ₃	17.66	2.655	2.512	2.519	2.518	2.871	3.099	1.018
K(Tren) ⁺	C ₃	58.19					2.831	2.849	1.018
Na(Tren) ₂	D ₃	33.24	2.184	2.008	2.012	2.011	2.639	3.148	1.019
Na(Tren) ₂ ⁺	D ₃	106.53					2.663	3.068	1.017
K(Tren) ₂	D ₃	33.12	2.122	1.953	1.959	1.959	2.950	3.205	1.019
K(Tren) ₂ ⁺	D ₃	85.93					2.975	2.160	1.017
Na(Azacrypt)	D ₃	22.74	1.863	1.768	1.767	1.767	2.769	3.343	1.019
Na(Azacrypt) ⁺	D ₃	103.43					2.771	3.362	1.019
K(Azacrypt)	D ₃	27.21	1.841	1.751	1.751	1.751	2.946	3.180	1.019
K(Azacrypt) ⁺	D ₃	86.51					2.965	3.191	1.018
Na(Tripip)	D ₃	25.89	1.783	1.694			2.678	3.099	
Na(Tripip) ⁺	D ₃	108.45					2.681	3.095	
K(Tripip)	D ₃	23.81	1.733	1.680			2.846	2.984	
K(Tripip) ⁺	D ₃	83.29					2.884	2.988	

^aN_e and N_a represent equatorial and axial N–atoms, respectively.

Excited state analysis of highly diffused complexes is known to be associated with great challenges.^{58,60,61} Especially, the predictions are sensitive to the quality of the utilizing level of theory and the basis sets. The EPT methods are proven to provide rather precise excitation energies for such systems.^{30,53,60} The accuracy and computational cost of EPT methods implemented in this work increases in the order of the KT < D2 < P3 < P3+. Indeed, the predictions of D2, P3, and P3+ methods on highly diffused systems are in great harmony with the state-of-art EOM-EA-CCSD (equation of motion coupled cluster singles and doubles method based on electron attachment) and CASPT2 (complete active space second-order perturbation theory).^{30,60,62} Our past benchmark studies support that the application of d-aug-cc-pVXZ (X = D, T) on the terminal H–atoms that directly interact with the diffuse electron cloud is crucial (see Refs. 53,54). On the other hand, application of cc-pVXZ (D, T) on the inner atoms is sufficient as an accuracy-efficiency compromise.^{53,54} In this work cc-pVDZ (M, C, N) d-aug-cc-pVDZ (H) basis set was selected to analyze excited states of all surface-type complexes.

Figure 2 provides the P3+ vertical excitation energies and the occupying Dyson orbitals of Na(Tren)₂. The singly occupied doughnut-shaped molecular orbital in the ground state is an approximate to a SA s-orbital (1S). In excited states this electron populates p-, d-, f-, and g-type orbitals (or SA P-, D-, F-, G-orbitals). Under D₃ symmetry the SA P-, D-, F-, and G-configurations split into {E and A₂}, {2E, A₁}, {2E, A₁, 2A₂}, and {3E, A₁, 2A₂} components, respectively. The first two electron transitions, i.e., 0.162 eV and 0.549 eV, correspond to SA 1P¹ configurations. The proceeding three excited states carry SA 1D¹ configurations (at 0.583, 0.744, and 0.760 eV). The SA 2S¹ (at 1.131 eV) lies among the splits of 1F¹ (1.078–1.167 eV). The second set of SA P-level populates at 1.274 eV and is followed by 1G¹ set (1.517–1.630 eV). In overall, the observed SA shell-model is 1S, 1P, 1D, 1F, 2S, 2P, and 1G. The calculated KT, D2, P3, and P3+ excitation energies of all M(Tren)₂, M(Azacrypt), and M(Tripip) (M = Na, K) are listed in Table 2. See SI for more information on their excitation energies. The excited states of K(Tren)₂ were also analyzed up to the 1G level and the shell model remains the same. All excitation energies of K(Tren)₂ are slightly lower compared to Na(Tren)₂ (by 0–0.070 eV), except for the 1P¹ (1²E) state which is higher by only 0.002 eV (see Tables S15 and S17). In this system only one component of 2P¹ (2²E) (at 1.224 eV) was identified as similar to Na(Tren)₂. Notice that the excited states of M(Azacrypt) and M(Tripip) (M = Na, K) were studied only up to 1F level due to the high computational cost. Comparatively, the computational cost of M(Tripip) is greater and hence only D2 level of theory was adopted. As a trend, excitation energies decrease moving from M(Tren)₂ to M(Azacrypt) and to M(Tripip) (compare values of Tables S15, S17, S19, S21, S23, and S25). Slightly lower excitation energies were observed for K(Azacrypt)/K(Tripip) (by 0–0.03 eV) compared to their Na-complexes.

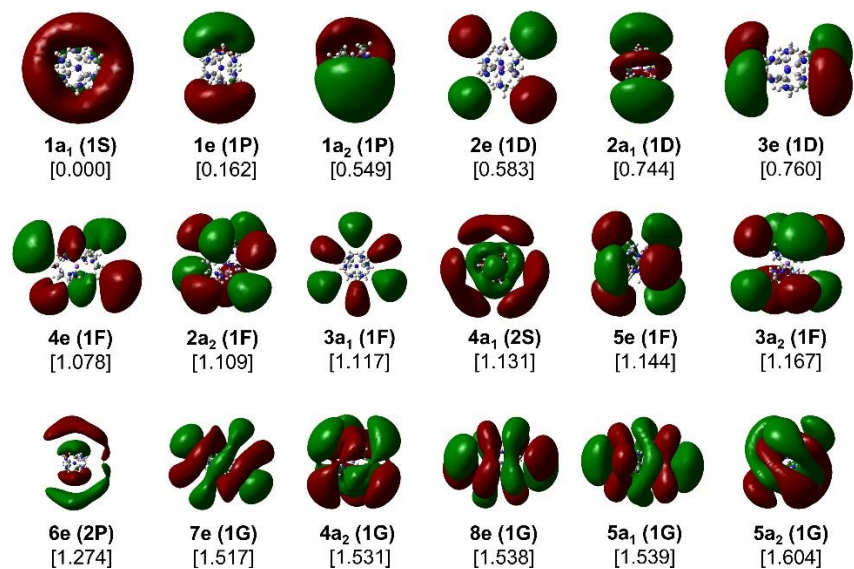


Figure 2. Representative Dyson orbitals for vertical electron attachment of $\text{Na}(\text{Tren})_2^+$ (D_3 point group). An isovalue of 0.02 a.u. was used. In each case the approximate SA shell is given in parenthesis. The P3+ vertical excitation energies (eV) are listed in square brackets.

Table 2. Vertical excitation energies (eV) of M(Tren)₂, M(Azacrypt), and M(Tripip) (M = Na, K) at EPT.

Approximate SA shell	KT	D2	P3	P3+
	Na(Tren) ₂			
1S	0.000	0.000	0.000	0.000
1P	0.122, 0.393	0.163, 0.553	0.162, 0.549	0.162, 0.549
1D	0.458–0.586	0.586–0.764	0.584–0.760	0.583–0.760
1F	0.883–0.930	1.080–1.172	1.078–1.168	1.078–1.167
2S	1.020	1.126	1.133	1.131
2P ^a	1.136	1.271	1.275	1.274
1G	1.274–1.379	1.518–1.631	1.518–1.631	1.517–1.630
K(Tren) ₂				
1S	0.000	0.000	0.000	0.000
1P	0.124, 0.379	0.164, 0.518	0.163, 0.516	0.164, 0.517
1D	0.445–0.568	0.570–0.722	0.568–0.720	0.569–0.721
1F	0.861–0.906	1.043–1.124	1.042–1.122	1.042–1.122
2S	0.975	1.057	1.064	1.064
2P ^a	1.111	1.219	1.224	1.224
1G	1.242–1.396	1.468–1.577	1.470–1.579	1.470–1.579
Na(Azacrypt)				
1S	0.000	0.000	0.000	0.000
1P	0.055, 0.238	0.014, 0.312	0.020, 0.303	0.019, 0.304
1D	0.381–0.450	0.464–0.550	0.458–0.543	0.459–0.543
1F	0.709–0.772	0.811–0.933	0.811–0.924	0.811–0.925
K(Azacrypt)				
1S	0.000	0.000	0.000	0.000
1P	0.045, 0.227	0.000, 0.298	0.006, 0.290	0.005, 0.291
1D	0.380–0.437	0.460–0.533	0.455–0.527	0.455–0.527
1F	0.695–0.759	0.803–0.914	0.802–0.907	0.802–0.907
Na(Tripip)				
1S	0.000			
1P	0.130, 0.223			
1D	0.432–0.476			
1F ^b	0.761–0.824			
K(Tripip)				
1S	0.000			
1P	0.128, 0.212			
1D	0.425–0.461			
1F ^b	0.734–0.815			

^a Within the focused energy range only one component of 2P¹ (6²E) was seen for Na(Tren)₂ and K(Tren)₂ (see Table S15 and S17). ^b Similarly, in the selected range only three components of 1F¹ (3²A₁, 4²E, and 2²A₂) were observed for Na(Tripip) and K(Tripip) (see Tables S23 and S25).

IIIB. M(Tren)₂@M', M(Azacrypt)@M', and M(Tripip)@M' (M/M' = Na, K) units

The diffuse electron of M(L)_n transfers to an incoming metal atom to produce a charge separated [M(L)_n]⁺@M'⁻. The D_{es} with respect to [M(L)_n@M']^{0,+} → [M(L)_n]^{0,+} + M' fragmentation of studied species are listed in Table 3. The D_{es} of neutral complexes decrease in the order of M(Azacrypt)@M' > M(Tripip)@M' > M(Tren)₂@M' for every studied metal atom combination. Similarly, the D_{es} varied in the series of K(L)_n@Na > Na(L)_n@Na > K(L)_n@K > Na(L)_n@K for all utilized ligand (L) types. Comparatively, the D_{es} of cationic complexes are significantly lower. The MP2 D_{es} were calculated only for neutral and cationic Na(L)₂@Na, Na(L)₂@K, K(L)₂@Na for L = Tren and their discrepancies with corresponding CAM-B3LYP values are less than 1.2 kcal/mol. As expected, the lower binding energy between [M(L)_n]⁺ + M' correlates to longer M...M distances of [M(L)_n@M']⁺, i.e., longer by 0.8–1.8 Å compared to their neutral units (Table 3). The largest ΔE_{S-T} were observed for the M(Azacrypt)@M' units, and they are higher for M' = Na compared to the M' = K cases (Table 3).

Going one step further the anions of Na(L)_n@Na were also studied at the D2 level of theory. The -VEAEs are reported in the Table 3. Note that there are two -VEAEs per each focused system which correspond to the ground and the first excited state of the anions. The computed electron affinities varied in the series of Na(Azacrypt)@Na < Na(Tripip)@Na < Na(Tren)₂@Na. In the ground state the radical electron of [Na(L)_n@Na]⁻ (1²A) occupies a polarized Rydberg-like orbital (~SA 1S) and its promotion to a SA 1P-orbital produces the first excited state (2²A) (Figure 3).

The lowest AIEs were observed for M(Tripip)@M' and the values are 0.6–1.0 eV higher compared to the respective M(Tripip) complexes (compare corresponding AIEs listed in Tables 1 and 3). The greater AIEs of M(L)_n@M' for M' = Na compared to M' = K correlates to the higher atomic electron affinity of the Na (0.548 eV) compared to K (0.501 eV).⁷ The MP2 AIEs are 0.1–0.3 eV lower compared to the CAM-B3LYP values. Indeed, according to Boldyrev's definition these alkali units too are superalkalis owing to their smaller IEs.^{31,32} The structures of cations bear [M(L)_n]⁺@M' form, where one radical electron is present at the exterior metal atom (M'). In the first three excited states this electron populates the atomic p-orbitals of M'. The energies related to these transitions and occupying orbitals are

given in Table S29 and Figure S1, respectively. Since the electron transition is almost perfect $s \rightarrow p$ of M' , the excitation energies of cationic units are expected to be comparable to the values of the bare M' -atoms. Indeed, the first three excitation energies of all $M' = \text{Na}$ and $M' = \text{K}$ cationic systems span within 1.992–2.160 and 1.425–1.591 eV, respectively, which are closer to the first excitation energies Na (2.10 eV) and K (1.61 eV).⁶³

Table 3. Dissociation energies (D_e , kcal/mol), equilibrium $M \cdots M$ distances (r_e , Å), vertical singlet-triplet energy gaps (ΔE_{S-T} , eV), negative of vertical electron attachment energies ($-VEAE$, eV), and adiabatic ionization energies (AIE, eV) of $[M(L)_n@M']^{0,+}$ systems.

Species	D_e^a	r_e	ΔE_{S-T}	$-VEAE$	AIE ^a
Na(Tren) ₂ @Na	20.29 (19.11)	5.500	0.511	0.411, 0.118	2.966 (2.691)
[Na(Tren) ₂ @Na] ⁺	2.28 (2.74)	6.357			
Na(Tren) ₂ @K	14.90 (14.28)	6.073	0.298		2.695 (2.431)
[Na(Tren) ₂ @K] ⁺	3.13 (3.91)	6.881			
K(Tren) ₂ @Na	21.35 (22.4)	4.791	0.616		2.955 (2.846)
[K(Tren) ₂ @Na] ⁺	2.13 (1.42)	6.548			
K(Tren) ₂ @K	15.40	5.806	0.320		2.661
[K(Tren) ₂ @K] ⁺	2.97	7.066			
Na(Azacrypt)@Na	27.49	4.771	0.642	0.240, 0.101	2.973
[Na(Azacrypt)@Na] ⁺	1.90	6.038			
Na(Azacrypt)@K	21.34	5.501	0.378		2.667
[Na(Azacrypt)@K] ⁺	2.80	6.559			
K(Azacrypt)@Na	27.62	4.968	0.641		2.958
[K(Azacrypt)@Na] ⁺	1.86	6.177			
K(Azacrypt)@K	21.45	5.699	0.386		2.653
[K(Azacrypt)@K] ⁺	2.73	6.662			
Na(Tripip)@Na	21.26	6.266	0.490	0.332, 0.135	2.643
[Na(Tripip)@Na] ⁺	1.41	7.158			
Na(Tripip)@K	16.39	6.848	0.302		2.412
[Na(Tripip)@K] ⁺	1.87	7.697			
K(Tripip)@Na	21.81	6.107	0.501		2.663
[K(Tripip)@Na] ⁺	2.68	7.152			
K(Tripip)@K	16.70	6.755	0.307		2.421
[K(Tripip)@K] ⁺	3.15	7.712			

^a MP2 D_e s and AIEs are given in parenthesis, whereas all other values obtained under CAM-B3LYP.

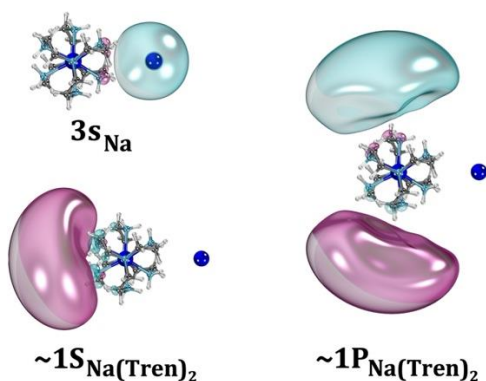


Figure 3. Selected orbitals of $[\text{Na}(\text{Tren})_2@Na]^-$. The $\sim 1S_{\text{Na}(\text{Tren})_2}$ and $\sim 1P_{\text{Na}(\text{Tren})_2}$ orbitals are singly occupied in 1^2A and 2^2A states of the $[\text{Na}(\text{Tren})_2@Na]^-$, respectively. The $3S_{\text{Na}}$ is doubly occupied in both states. Orbitals of 1^2A and 2^2A of $[\text{Na}(\text{Azacrypt})@Na]^-$ and $[\text{Na}(\text{TriPIP})@Na]^-$ have similar shapes.

IV. Conclusions

The ground and electronically excited states of $M(L)_n$ ($M = \text{Na}, \text{K}$; $L = \text{Tren}, \text{Azacryptand}, \text{TriPIP222}$; $n = 1, 2$) molecular electriles and their analogous alkali complexes, $M(L)_n@M'$, were analyzed using *ab initio* methods. The complexes are stable with respect to their corresponding $M(L)_n \rightarrow M + nL$ and $M(L)_n@M' \rightarrow M(L)_n + M'$ dissociations. In the ground state the $M(L)_n$ carries a diffuse electron in the periphery which occupies atomic-type orbitals in excited states. Consequently, they were identified as superatoms. The superatomic (SA) shell model discovered for $M(\text{Tren})_2$ is 1S, 1P, 1D, 1F, 2S, 2P, and 1G. This orbital order is similar to the trends we have seen in the past for similar diffused systems. Due to the high computational cost the excited states of $M(\text{Azacryptand})$ and $M(\text{TriPIP222})$ were studied only up to the 1F level, and the order is consistent with that of $M(\text{Tren})_2$. The excitation energies and ionization energies decreased moving from $M(\text{Tren})_2$ to $M(\text{Azacryptand})$ and to $M(\text{TriPIP222})$, and the trend correlates to the number of N-H terminals in them, which tends to stabilize Rydberg-like electrons. The reaction between $M(L)_n$ and M' causes an electron transfer from the former to the latter producing a charge separated structure for alkali units, i.e., $[M(L)_n]^+@M'^-$ (M' carries two electrons in the valence *ns*-orbital). The D_{eS} of $M(L)_n@M'$ decreased in the sequence of $M(\text{Azacryptand})@M' > M(\text{TriPIP222})@M' > M(\text{Tren})_2@M'$ (for all M and M' combinations) and $K(L)_n@Na >$

$\text{Na}(\text{L})_n @ \text{Na} > \text{K}(\text{L})_n @ \text{K} > \text{Na}(\text{L})_n @ \text{K}$ (for all L). The radical electron occupies the valence ns -orbital of M' of $[\text{M}(\text{L})_n @ \text{M}']^+$ which promotes to its np - and $(n+1)s$ -orbitals in excited states. Similar to $\text{M}(\text{L})_n$, in $[\text{Na}(\text{L})_n @ \text{Na}']^-$ the radical electron occupies diffuse SA 1S- and 1P-orbitals in the ground and the first excited state.

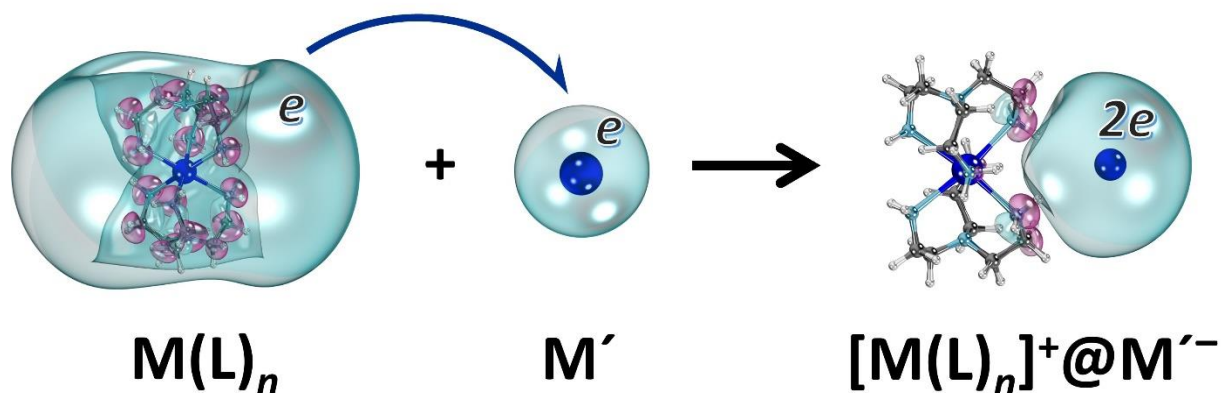
Conflicts of interest

There are no conflicts to declare.

Acknowledgements

This work was completed with the resources provided by the Alabama supercomputer and the National Energy Research Scientific Computing Center (NERSC), a U.S. Department of Energy Office of Science User Facility operated under Contract No. DE-AC02-05CH11231.

TOC Graphics



References

- 1 X. Zhang and G. Yang, *J. Phys. Chem. Lett.*, 2020, **11**, 3841–3852.
- 2 C. Liu, S. A. Nikolaev, W. Ren and L. A. Burton, *J. Mater. Chem. C*, 2020, **8**, 10551–10567.
- 3 M.-S. Miao and R. Hoffmann, *Acc. Chem. Res.*, 2014, **47**, 1311–1317.
- 4 S. G. Dale, A. D. Becke and E. R. Johnson, *Phys. Chem. Chem. Phys.*, 2018, **20**, 26710–

- 26718.
- 5 M. J. Wagner and J. L. Dye, *Annu. Rev. Mater. Sci.*, 1993, **23**, 223–253.
 - 6 M. J. Wagner and J. L. Dye, in *Molecular Recognition: Receptors for Cationic Guests*, ed. G. W. Gokel, Pergamon, Oxford, UK, 1st edn., 1996, pp. 477–510.
 - 7 D. R. Lide, *CRC Handbook of Chemistry and Physics*, CRC press, New York, 93rd edn., 2012.
 - 8 K. Lee, S. W. Kim, Y. Toda, S. Matsuishi and H. Hosono, *Nature*, 2013, **494**, 336–340.
 - 9 J. L. Dye, *Science (80-.)*, 2003, **301**, 607–608.
 - 10 R. Riedel, A. G. Seel, D. Malko, D. P. Miller, B. T. Sperling, H. Choi, T. F. Headen, E. Zurek, A. Porch, A. Kucernak, N. C. Pyper, P. P. Edwards and A. G. M. Barrett, *J. Am. Chem. Soc.*, 2021, **143**, 3934–3943.
 - 11 H. Hosono and M. Kitano, *Chem. Rev.*, 2021, **121**, 3121–3185.
 - 12 N. Davison, J. A. Quirk, F. Tuna, D. Collison, C. L. McMullin, H. Michaels, G. H. Morritt, P. G. Waddell, J. A. Gould, M. Freitag, J. A. Dawson and E. Lu, *Chem*, 2023, **9**, 576–591.
 - 13 J. Mai, S. Gong, N. Li, Q. Luo and Z. Li, *Phys. Chem. Chem. Phys.*, 2015, **17**, 28754–28764.
 - 14 S. G. Dale and E. R. Johnson, *J. Phys. Chem. A*, 2018, **122**, 9371–9391.
 - 15 S. Guan, S. Y. Huang, Y. Yao and S. A. Yang, *Phys. Rev. B*, 2017, **95**, 165436.
 - 16 H.-M. He, Y. Li, H. Yang, D. Yu, S.-Y. Li, D. Wu, J.-H. Hou, R.-L. Zhong, Z.-J. Zhou, F.-L. Gu, J. M. Luis and Z.-R. Li, *J. Phys. Chem. C*, 2017, **121**, 958–968.
 - 17 D. J. Singh, H. Krakauer, C. Haas and W. E. Pickett, *Nature*, 1993, **365**, 39–42.
 - 18 E. Zurek, *J. Am. Chem. Soc.*, 2011, **133**, 4829–4839.
 - 19 S. G. Dale, A. Otero-de-la-Roza and E. R. Johnson, *Phys. Chem. Chem. Phys.*, 2014, **16**, 14584–14593.
 - 20 S. G. Dale and E. R. Johnson, *Phys. Chem. Chem. Phys.*, 2017, **19**, 27343–27352.
 - 21 S. G. Dale and E. R. Johnson, *Phys. Chem. Chem. Phys.*, 2017, **19**, 12816–12825.
 - 22 I. R. Ariyaratna and E. Miliordos, *Phys. Chem. Chem. Phys.*, 2021, **23**, 20298–20306.
 - 23 I. R. Ariyaratna, *Inorg. Chem.*, 2022, **61**, 579–585.
 - 24 B. A. Jackson, S. G. Dale, M. Camarasa-Gómez and E. Miliordos, *J. Phys. Chem. C*, 2023, **127**, 9295–9308.
 - 25 P. Jena and Q. Sun, *Chem. Rev.*, 2018, **118**, 5755–5870.

- 26 I. R. Ariyaratna, *Int. J. Quantum Chem.*, 2021, **121**, 1–9.
- 27 I. R. Ariyaratna, *Phys. Chem. Chem. Phys.*, 2021, **23**, 18588–18594.
- 28 I. R. Ariyaratna, F. Pawłowski, J. V. Ortiz and E. Miliordos, *Phys. Chem. Chem. Phys.*, 2018, **20**, 24186–24191.
- 29 I. R. Ariyaratna and E. Miliordos, *Phys. Chem. Chem. Phys.*, 2019, **21**, 15861–15870.
- 30 I. R. Ariyaratna and E. Miliordos, *Phys. Chem. Chem. Phys.*, 2020, **22**, 22426–22435.
- 31 G. L. Gutsev and A. I. Boldyrev, *Chem. Phys. Lett.*, 1982, **92**, 262–266.
- 32 N. V. Tkachenko, Z.-M. Sun and A. I. Boldyrev, *ChemPhysChem*, 2019, **20**, 2060–2062.
- 33 IUPAC name of Azacryptand: 1,4,7,10,13,16,21,24-octaazabicyclo[8.8.8]hexacosane.
- 34 IUPAC name of TriPip222: 1,4,7,10,13,16,21,24-octaazapentacyclo[8.8.8.24,7.213,16.221,24]dotriacontane.
- 35 T. Yanai, D. P. Tew and N. C. Handy, *Chem. Phys. Lett.*, 2004, **393**, 51–57.
- 36 B. P. Prascher, D. E. Woon, K. A. Peterson, T. H. Dunning and A. K. Wilson, *Theor. Chem. Acc.*, 2011, **128**, 69–82.
- 37 R. A. Kendall, T. H. Dunning and R. J. Harrison, *J. Chem. Phys.*, 1992, **96**, 6796–6806.
- 38 C. Lee, W. Yang and R. G. Parr, *Phys. Rev. B*, 1988, **37**, 785–789.
- 39 A. D. Becke, *J. Chem. Phys.*, 1993, **98**, 5648–5652.
- 40 P. J. Stephens, F. J. Devlin, C. F. Chabalowski and M. J. Frisch, *J. Phys. Chem.*, 1994, **98**, 11623–11627.
- 41 S. H. Vosko, L. Wilk and M. Nusair, *Can. J. Phys.*, 1980, **58**, 1200–1211.
- 42 C. Møller and M. S. Plesset, *Phys. Rev.*, 1934, **46**, 618–622.
- 43 T. Koopmans, *Physica*, 1934, **1**, 104–113.
- 44 J. Linderberg and Y. Öhrn, *Propagators in Quantum Chemistry*, John Wiley & Sons, New Jersey, 2004.
- 45 J. V. Ortiz, *Int. J. Quantum Chem.*, 2005, **105**, 803–808.
- 46 J. V. Ortiz, *Wiley Interdiscip. Rev. Comput. Mol. Sci.*, 2013, **3**, 123–142.
- 47 H. H. Corzo and J. V. Ortiz, 2017, pp. 267–298.
- 48 G. Knizia, *J. Chem. Theory Comput.*, 2013, **9**, 4834–4843.
- 49 G. Schaftenaar and J.H. Noordik, *J. Comput. Aided. Mol. Des.*, 2000, **14**, 123–134.
- 50 R. Dennington, T. A. Keith and J. M. Millam, Shawnee Mission KS, 2016.
- 51 T. Tsurusawa and S. Iwata, *J. Phys. Chem. A*, 1999, **103**, 6134–6141.

- 52 B. M. Reinhard and G. Niedner-Schatteburg, *Phys. Chem. Chem. Phys.*, 2002, **4**, 1471–1477.
- 53 I. R. Ariyaratna, F. Pawłowski, J. V. Ortiz and E. Miliordos, *J. Phys. Chem. A*, 2020, **124**, 505–512.
- 54 I. R. Ariyaratna, S. N. Khan, F. Pawłowski, J. V. Ortiz and E. Miliordos, *J. Phys. Chem. Lett.*, 2018, **9**, 84–88.
- 55 I. R. Ariyaratna and E. Miliordos, *J. Comput. Chem.*, 2019, **40**, 1344–1351.
- 56 I. R. Ariyaratna and E. Miliordos, *J. Comput. Chem.*, 2019, **40**, 1740–1751.
- 57 I. R. Ariyaratna, N. M. S. Almeida and E. Miliordos, *J. Phys. Chem. A*, 2019, **123**, 6744–6750.
- 58 N. M. S. Almeida and E. Miliordos, *Phys. Chem. Chem. Phys.*, 2019, **21**, 7098–7104.
- 59 M. Y. Redko, J. E. Jackson, R. H. Huang and J. L. Dye, *J. Am. Chem. Soc.*, 2005, **127**, 12416–12422.
- 60 N. M. S. Almeida, F. Pawłowski, J. V. Ortiz and E. Miliordos, *Phys. Chem. Chem. Phys.*, 2019, **21**, 7090–7097.
- 61 S. N. Khan and E. Miliordos, *J. Phys. Chem. A*, 2020, **124**, 4400–4412.
- 62 I. R. Ariyaratna, *Phys. Chem. Chem. Phys.*, 2021, **23**, 16206–16212.
- 63 A. Kramida, Y. Ralchenko, J. Reader and NIST ASD Team., NIST Atomic Spectra Database (version 5.4), National Institute of Standards and Technology, Gaithersburg, MD 2016, <http://physics.nist.gov/asd>, (accessed 23 June 2023).